Applied Surface Science 255 (2009) 7234–7237

Contents lists available at ScienceDirect

Applied Surface Science

journal homepage: www.elsevier.com/locate/apsusc

Characterization of ceria–yttria stabilized zirconia plasma-sprayed coatings

Bin Ma, Yao Li *, Ke Su

Center for Composite Materials, Harbin Institute of Technology, No. 2 Yikuang Street, Nangang District, Harbin 150080, PR China

ARTICLE INFO

Article history:
Received 19 December 2008
Received in revised form 22 March 2009
Accepted 22 March 2009
Available online 31 March 2009

Keywords:
Ceria–yttria stabilized zirconia coatings
XPS
XRD

ABSTRACT

Ceria–yttria stabilized zirconia (CYSZ) coatings were prepared by air plasma-sprayed on the nickel alloy. The as-sprayed CYSZ coatings and heat-treated CYSZ coatings were characterized by X-ray photoelectron spectroscopy (XPS) and X-ray diffraction (XRD). The XPS data indicated the coexistence of Ce^{3+}, Ce^{4+}, Y^{3+} and Zr^{4+} ions near the surface of the as-sprayed CYSZ coatings and the disappearance of Ce^{3+} ions in the CYSZ coatings after thermal treatment at 1000 °C for 15 h. From the XRD patterns, the solid solution of CeO_2–Y_2O_3–ZrO_2 formed in the CYSZ coatings because of the lack of any features from Y_2O_3 and ZrO_2 single phases. After thermal treatment, the main phases of all the samples were consistent with the characteristic peaks of cubic ZrO_2.

1. Introduction

Stabilized Zirconia has been actively investigated because of a variety of applications, such as thermal barrier coatings (TBCs), oxygen sensors and solid oxide fuel cells (SOFC). It is known that below 1170 °C the stable phase of bulk zirconia is monoclinic, while from 1170 to 2370 °C the stable phase is tetragonal. Above 2370 °C the stable phase is cubic. But the tetragonal and the cubic phases can be stabilized near room temperature by doping trivalent and divalent metal oxides into the zirconia. Many metal oxides such as Y_2O_3, CeO_2, CaO, MgO, Yb_2O_3, Gd_2O_3, Al_2O_3, Ta_2O_5, HfO_2 and La_2O_3 are dopants into zirconia [1–11]. At moderate operation temperatures, the best compromise satisfying most of the above requirements is presently offered by 8 wt.% Y_2O_3–ZrO_2 (8YSZ) on a MCrAlY (M = Ni, Co) bond coat, deposited either by air plasma spraying (APS) or by electro-beam physical vapor deposition (EB-PVD). With respect to 8YSZ coatings, CeO_2–ZrO_2 coatings exhibit an improved thermal shock resistance, a better corrosion resistance and a lower thermal conductivity [12–14]. By way of contrast, a lower phase composition stability has been evidenced. At high temperatures, ceria doped zirconia is an electron–oxygen ion mixed conducting material because of the valence change between Ce^{4+} and Ce^{3+}. The reaction is represented using the Kröger–Vink notation [15],

$$2Ce_{Zr}^{X} + O_{o}^{X} \leftrightarrow 2Ce'_{Zr} + V''_{o} + \frac{1}{2}O_2 \quad (1)$$

As the expression (1), though the oxygen vacancies appear which is in favor of the thermal insulating properties, the phase stability become lower. In order to overcome this problem, the combined use of CeO_2 and Y_2O_3 as stabilizers could represent a possible compromise solution, ensuring the good features of both stabilizers with a probable synergic effect.

In this work, CeO_2 was incorporated into 7YSZ to improve the corrosion resistance, fracture toughness, and thermal insulation of the coatings. CYSZ coatings were prepared by air plasma-sprayed on the nickel alloy. XPS were used to examine the chemical and electron states of the as-sprayed CYSZ coatings and thermal-treated CYSZ coatings.

The crystal structure of samples was investigated by XRD.

2. Experimental details

The CYSZ coatings were deposited by a commercial air plasma spray (APS) equipment. The main chemicals used in this work were CeO_2 (99.9%, Aldrich) and 7 wt.% Y_2O_3 stabilized ZrO_2 (7YSZ) (99.9%, Aldrich). The starting powders for plasma-sprayed were obtained by mixing CeO_2 and 7YSZ powders with the molar ratio of 1:9 by magnetic mixer. The size of the CeO_2 powders is from 20 μm to 100 μm, and the size of the 7YSZ powders is from 35 μm to 75 μm. The micro-7YSZ powders are made by nano-7YSZ powders with the size of 12–25 nm. The nickel alloy substrates were cleaned, dried and grit sprayed. The CYSZ coatings were deposited with a 300 μm thick on the substrates then naturally cooled to room temperature. Some samples were thermally treated at 1000 °C for 15 h. Then the samples were cut into small plates with the dimensions of 10 mm length × 10 mm width for measurements.

The XPS measurements were performed on a PHI ESCA 5700 X-ray Photoelectron Spectrometer at the base pressure of about 8×10^{-10} Torr. The present X-ray source was Al Ka (1486.6 eV)

* Corresponding author. Tel.: +86 451 86402345; fax: +86 451 86402345.
E-mail address: liyao@hit.edu.cn (Y. Li).

0169-4332/$ – see front matter © 2009 Elsevier B.V. All rights reserved.
doi:10.1016/j.apsusc.2009.03.071

radiation. The core level spectra of Ce 3d, Zr 3d, Y 3d and O 1s were acquired with the pass energy of 29.35 eV and a step of 0.125 eV per channel. XPS surveys were also carried out after argon ion (Ar^+) bombardment of the samples. All recorded lines were calibrated to the C 1s line. The atomic percentages of Ce, Zr, Y and O are respectively calculated from the peak areas and sensitivity factors by

$$X\% = \frac{(A_X/S_X)}{\sum_{i=1}^{N}(A_X/S_X)} \quad (2)$$

where X is the element, A_X is the area under the peak for element X in the spectrum, and S_X is the sensitivity factor.

The crystalline phases of the samples were identified by powder X-ray diffraction on a Rigaku D/max-rB X-ray diffractometer with Cu Kα radiation of 1.5418 Å. The X-ray tube was operated at 40 kV and 50 mA. The X-ray diffractogram was recorded at 0.02° intervals in the range of 10–90° with a scanning velocity of 5° min^{-1}.

3. Results and discussion

The XPS method was used to examine the probable changes in electronic states and chemical environment of the Ce, Zr, Y and O atoms in the CYSZ coatings coated on the nickel alloy plates.

Fig. 1a–d shows the Ce 3d, Zr 3d, Y 3d and O 1s photoelectron spectra of CYSZ coatings. And Table 1 lists the core level binding energies measured in selected elements.

Fig. 1a shows Ce $3d_{5/2}$ and Ce $3d_{3/2}$ photoelectron spectra obtained in the two samples which are un-treated as coated and heat treated at 1000 °C for 15 h. Six peaks labeled as V_0, V_1, V_2 ($3d_{5/2}$), V'_0, V'_1 and V'_2 ($3d_{3/2}$) referring to three pairs of spin–orbit doublets can be identified and they are characteristic of Ce^{4+} 3d final states. And the spin–orbit doublet u/u' is corresponding to Ce^{3+} 3d final state [16]. The doublet V_0/V'_0 at 882.4 and 900.8 eV from as-sprayed coatings and the doublet V_0/V'_0 at 882.4 and 900.9 eV from heat-treated coatings are corresponding to Ce(IV)$3d^9 4f^1 O2p^4$ final state. And the doublet V_1/V'_1 at 888.8 and 907.4 eV from heat-treated coatings are assigned to the final state of Ce(IV)$3d^9 4f^1 O2p^5$. The high binding energy doublet V_2/V'_2 at 898.5 and 916.7 eV from as-sprayed coatings and the doublet V_2/V'_2 at 898.4 and 916.6 eV from heat-treated coatings are attributed to the final state of Ce(IV)$3d^9 4f^0 O2p^6$. The doublet u/u' at 885.3 and 903.9 eV are originated from the state of Ce(III)$3d^9 4f^2 O2p^5$. Compared with literature results, which were tested in independent samples, it reveals that the Ce^{4+} plus Ce^{3+} species coexist in the as-sprayed samples, whereas Ce^{4+} ions are only contained in the heat-treated samples [17–19]. The binding energies of Ce $3d_{5/2}$ lying at 885.3 eV and Ce $3d_{3/2}$ lying at 903.9 eV are the Ce^{3+} component. The cerium ion presenting in the trivalent state gives rise to high oxygen vacancy concentrations with an increased stability effect. In particular, the presence of Ce_2O_3 tends to stabilize a cubic zirconia with pyroclore structure [20]. The thermal treatment causes complete oxidation of Ce^{3+} to Ce^{4+} transformation, as evidenced by XPS spectra.

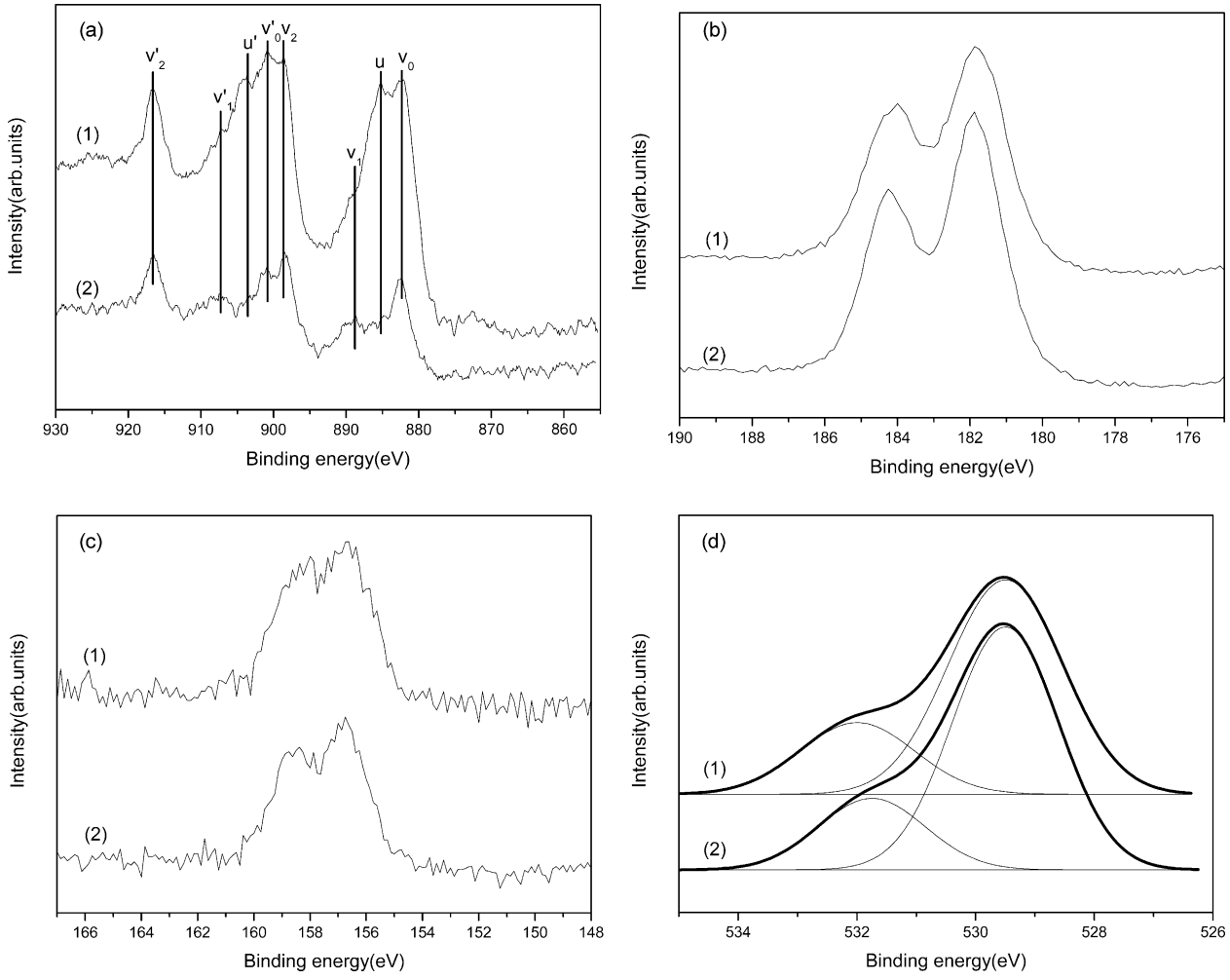

Fig. 1. XPS spectra of (a) Ce 3d doublet, (b) Zr 3d doublet, (c) Y 3d doublet and (d) O 1s in CYSZ coatings with different conditions (as marked in Table 1).

Table 1
XPS data for CYSZ coatings.

No.	Samples	Condition	Ce $3d_{5/2}$ (eV)	Ce $3d_{3/2}$ (eV)	Zr $3d_{3/2}$ (eV)	Y $3d_{3/2}$ (eV)	O 1s (eV)
1	CYSZ	As-sprayed	882.4, 885.3, 898.5	900.8, 903.9, 916.7	181.8	156.6	529.6, 532.0
2	CYSZ	Treated at 1000 °C for 15 h	882.4, 888.8, 898.4	900.9, 907.4, 916.6	181.8	156.7	529.5, 531.8

Table 2
The atomic composition of CYSZ coatings obtained from XPS analysis.

No.	Samples	Condition	Ce 3d (at.%)	Zr 3d (at.%)	Y 3d (at.%)	O 1s (at.%)
1	CYSZ	As-sprayed	8	19	2	71
2	CYSZ	Treated	3	22	3	72

In Fig. 1b and c, there is no apparent difference in the Zr 3d and Y 3d spectra between the two kinds of samples. The spectra for the O 1s ionization feature are numerically fitted with two Gaussian–Lorenz features, which are shown in Fig. 1d. The primary binding energy (BE) peak between 529.5 ± 0.2 eV represents the O 1s ionization for oxygen associated with the ceria–yttria–zirconia mixed oxides [21]. The higher binding energy features suggest the formation of Ce(III) related surface defects, where oxygen occupies additional lattice sites like vacancy or oxide ions in a defective CeO_x ($x < 2$), or oxygen chemisorbed on the surface in other forms such as CO, CO_2, or water or –OH species [22–25].

The atomic percentage of the composition in the CYSZ coatings is determined using sensitivity factors of 204.92, 60.06, 50.57 and 17.43 for Ce 3d, Zr 3d, Y 3d and O 1s, respectively. In light of the expression (2), the atomic percentages of Ce, Zr, Y and O are respectively calculated from the peak areas and sensitivity factors. The atomic percentages of elements in the CYSZ coatings are summarized in Table 2. Compared with molar ratio in the starting powders, it is easily to be found that the content of Ce element reduces. The reason is the evaporation of CeO_2 during air plasma spraying.

Fig. 2 shows the XRD patterns of CYSZ starting powders, CYSZ coatings as-sprayed and CYSZ coatings heat-treated at 1000 °C for 15 h. The main peaks of XRD patterns of all the samples are consistent with the characteristic peaks of cubic ZrO_2 while presenting superiority in symmetry. In Fig. 2a, the cubic ZrO_2 and cubic CeO_2 are only contained in the CYSZ starting powders, which reveals that Y_2O_3 and ZrO_2 form the solid solution completely in the 8YSZ powders. In Fig. 2b and c, the cubic CeO_2 phase disappears. And a small amount of $Ce_{1-x}Zr_xO_2$ ($0 < x < 1$) phase is visible in the Fig. 2b and c. From the XRD patterns, the solid solution of CeO_2–Y_2O_3–ZrO_2 formed in the CYSZ coatings because of the lack of any features from Y_2O_3 and ZrO_2 single phases. The main peaks experience a sharpening after thermal treatment, which indicates the growth and integrity of crystal grain. The formation of the cubic phase of ZrO_2 based solid solutions depends on the amount of dopant as well as the treatment temperature. The small shift of diffraction peaks with respect to pure cubic ZrO_2 is a result of Y and/or Ce incorporation. As shown in Fig. 3, the (1 1 1) peak of CYSZ coatings as-sprayed shifts to the smaller degree region. The angular region 28.6° and 31° in 2θ, encompassing the (1 1 1) peak of cubic ZrO_2, was studied for qualitative analysis of the phases present. The results of peak separation of CYSZ coatings as-sprayed in the (1 1 1) peak region are shown in Fig. 4. The 1 peak is the (1 1 1) peak of the as-sprayed CYSZ coatings and 2–6 peaks are separated peaks from the original peak 1. The peaks of 2, 3, 4, 5,

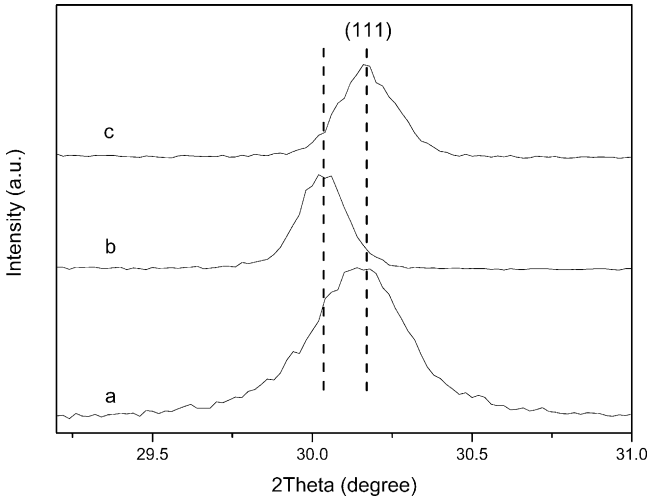

Fig. 3. XRD patterns of the (1 1 1) peak region of (a) CYSZ starting powders, (b) CYSZ coatings as-sprayed and (c) CYSZ coatings treated at 1000 °C for 15 h.

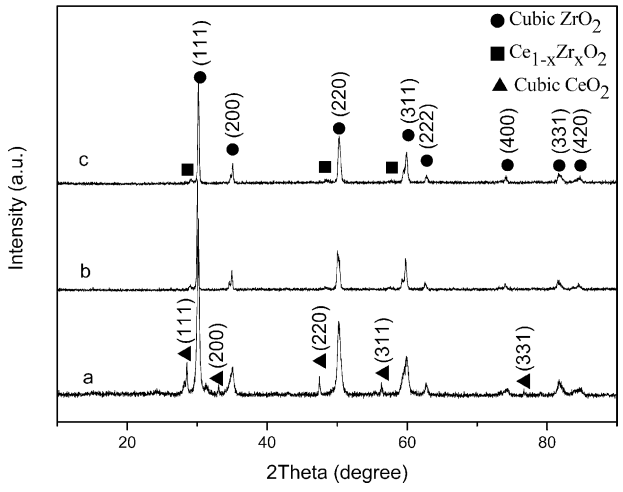

Fig. 2. XRD patterns of (a) CYSZ starting powders, (b) CYSZ coatings as-sprayed and (c) CYSZ coatings treated at 1000 °C for 15 h.

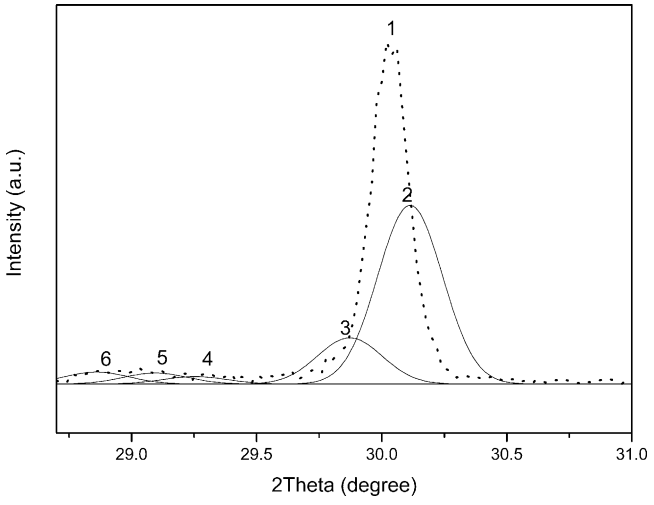

Fig. 4. The results of peak separation of CYSZ coatings as-sprayed in the (1 1 1) peak region.

and 6 are corresponded to the (1 1 1) peak of cubic ZrO_2, (1 0 1) peak of $Zr_{0.84}Ce_{0.16}O_2$, (1 0 1) peak of $Zr_{0.5}Ce_{0.5}O_2$, (1 1 1) peak of $Zr_{0.4}Ce_{0.6}O_2$ and (1 1 1) peak of $Zr_{0.25}Ce_{0.75}O_2$, respectively.

The outer electron configuration of Ce, Y and Zr atom is $4f^15d^16s^2$, $4d^15s^2$ and $4d^25s^2$, respectively. Because of a large similarity in the ionic radii between Ce^{3+} (1.03 Å), Y^{3+} (0.89 Å), Ce^{4+} (0.92 Å) and Zr^{4+} (0.79 Å), it is easy to form a new compound when the two materials mixed in a certain temperature. From the ionic radii of metal in the CYSZ coatings, the Zr^{4+} is the smallest. Metal ions larger than Zr^{4+} are especially effective in stabilizing the cubic phase [26]. Because the starting powders are mixed by a mechanical method, the composition distribution is uneven. While in the spraying process, most of the starting powders are in melting phase. When Ce^{4+} ions enter into the lattice of ZrO_2, the solid solution of $Ce_{1-x}Zr_xO_2$ ($x \geq 0.5$) generate. But Zr^{4+} ions filter into the lattice of CeO_2 in the CeO_2 rich area, the solid solution of $Ce_{1-x}Zr_xO_2$ ($x \leq 0.5$) will form. After spraying the temperature of the coatings drops very quickly, multi-phase solid solutions coexist in the CYSZ coating. When the CYSZ coatings are thermally treated at high temperature for a long time, the Ce^{4+} ions can enter into the lattices and defects of ZrO_2 completely. The samples thermally treated are crystallized better. The main peaks of CYSZ coatings shift to the locations of the peaks of cubic ZrO_2 after thermal treatment as shown in the Figs. 2 and 3.

4. Conclusion

The present XPS and XRD investigations show that the CeO_2–Y_2O_3–ZrO_2 solid solutions form in the as-sprayed CYSZ coatings on the nickel alloy substrate. After thermal treatment at 1000 °C for 15 h, the main phases of all the samples are consistent with the characteristic peaks of cubic ZrO_2. The metal ions of Ce^{3+}, Ce^{4+}, Y^{3+} and Zr^{4+} appear on the surface of the as-sprayed CYSZ coatings, but the trivalent Ce cations disappear in the thermal-treated CYSZ coatings.

Acknowledgments

We thank the National Natural Science Foundation of China (No. 20601006), Program for New Century Excellent Talents in University (NCET-06-0335), Natural Scientific Research Innovation Foundation in HIT (200804) and CAST Foundation for financial support.

References

[1] U. Schulz, K. Fritscher, C. Leyens, Surf. Coat. Technol. 133–134 (2000) 40–48.
[2] F.M. Pitek, C.G. Levi, Surf. Coat. Technol. 201 (2007) 6044–6050.
[3] C. Leyens, U. Schulz, K. Fritscher, Mater. High Temp. 20 (2003) 475–480.
[4] J. Zhang, A. Kobayashi, Vacuum 83 (2008) 92–97.
[5] A.E. Nelson, K.H. Schulz, Appl. Surf. Sci. 210 (2003) 206–221.
[6] E. Celik, I. Birlik, Y. Karakas, J. Mater. Process. Tech. 209 (2009) 695–699.
[7] W. Ma, D. Mack, J. Malzbender, J. Eur. Ceram. Soc. 28 (2008) 3071–3081.
[8] X. Zhang, P. Hu, Scripta. Mater. 57 (2007) 1036–1039.
[9] W. Ma, S. Gong, H. Xu, Surf. Coat. Technol. 200 (2006) 5113–5118.
[10] X. Cao, R. Vassen, W. Fischer, Adv. Mater. 15 (2003) 1438–1441.
[11] K. Matsumoto, Y. Itoh, T. Kameda, Sci. Technol. Adv. Mater. 1544 (2003) 153–158.
[12] J.R. Brandon, R. Taylor, Surf. Coat. Technol. 39–40 (1989) 143–151.
[13] D.Q. Peng, X.D. Bai, Q.G. Zhou, J. Nucl. Mater. 324 (2004) 71–75.
[14] S.Y. Park, J.H. Kim, M.C. Kim, Surf. Coat. Technol. 190 (2005) 357–365.
[15] T. Otake, H. Yugami, H. Naito, Solid State Ionics 135 (2000) 663–667.
[16] L. Qiu, F. Liu, L. Zhao, Y. Ma, J. Yao, Appl. Surf. Sci. 252 (2006) 4931–4935.
[17] A. Dauscher, L. Hilaire, F. LeNormand, Surf. Interface Anal. 16 (1990) 341–346.
[18] T.L. Barr, C.G. Fries, F. Cariati, J. Phys. Chem. 82 (1978) 1801–1810.
[19] E. Beche, P. Charvin, D. Perarnan, Surf. Interface Anal. 40 (2008) 264–267.
[20] R.D. Maschio, P. Scardi, L. Lutterotti, J. Mater. Sci. 27 (1992) 5591–5596.
[21] I. Avramova, D. Stoychev, Ts. Marinova, Appl. Surf. Sci. 253 (2006) 1365–1370.
[22] A. Pfau, K.D. Schierbaum, Surf. Sci. 321 (1994) 71–80.
[23] D.R. Mullins, S.H. Overbury, D.R. Huntley, Surf. Sci. 409 (1998) 307–319.
[24] K. Schierbaum, Surf. Sci. 399 (1998) 29–38.
[25] A.E.C. Palmqvist, M. Wirde, U. Gelius, Nanostruct. Mater. 11 (1999) 995–1007.
[26] P. Li, I.W. Chen, Phys. Rev. B 48 (1993) 10074–10081.